Experiments in Fluids 16, 82–96 (1993)

Experiments in Fluids

Measurements of thermally stratified pipe flow using image-processing techniques

J. Sakakibara, K. Hishida, M. Maeda

Department of Mechanical Engineering, Keio University, 3-14-1 Hiyoshi, Kohoku-ku, Yokohama 223, Japan

Received: 15 October 1992 / Accepted: 4 March 1993

Abstract. The cross-correlation technique and Laser Induced Fluorescence (LIF) have been adopted to measure the time-dependent and two-dimensional velocity and temperature fields of a stably thermal-stratified pipe flow. One thousand instantaneous and simultaneous velocity and temperature maps were obtained at overall Richardson number $Ri=0$ and 2.5, from which two-dimensional vorticity, Reynolds stress and turbulent heat flux vector were evaluated. The quasi-periodic inclined vortices (which connected to the 'crest') were revealed from successive instantaneous maps and temporal variation of vorticity and temperature. It has been recognized that these vortices are associated with the 'crest' and 'valley' in the roll-up motion.

List of symbols

A	Fraction of the available light collected
C	Concentration of fluorescence
D	Pipe diameter
I	Fluorescence intensity
L	Sampling length along the incident beam
I_0	Intensity of an excitation beam
$I_c(T)$	Calibration curve between temperature and fluorescence intensity
I_{ref}	Reference intensity of fluorescence radiation
Re_b	Reynolds number based on bulk velocity, U_bD/ν
Ri	Overall Richardson number based on velocity difference, $\beta g D\Delta T/\Delta U^2$
t	Time
Δt	Time interval between the reference and corresponding matrix
T	Temperature
T_1, T_2	Temperature of lower and upper layer
T^*	Normalized temperature, $(T-T_1)/\Delta T$
$T_c(I)$	Inverse function of temperature as a function of I_c
T_{ref}	Reference temperature
ΔT	Temperature difference between upper and lower flow, T_2-T_1
U_1	Velocity of lower stream
U_2	Velocity of upper stream
U_b	Bulk velocity
U_c	Streamwise mean velocity at $Y/D=0$
ΔU	Streamwise velocity difference between upper and lower flow, U_1-U_2
u', v', T'	Fluctuating component of U, V, T
U, V	Velocity component of X, Y direction
X	Streamwise distance from the splitter plate
Y	Transverse distance from the centerline of the pipe
Z	Spanwise distance from the centerline of the pipe
ϕ	Quantum yield
ε	Absorptivity
ω	vorticity calculated from a circulation
ν	Kinematic viscosity
Γ	circulation

Correspondence to: J. Sakakibara

1 Introduction

Heat and momentum transfer in pipe flow accompanying thermal buoyancy as an active scalar, such as a thermal-stratified flow is encountered in many technological systems. In the stable thermally stratified pipe flow, the temperature difference between upper and lower layers yields a buoyancy force, which suppresses the momentum and/or heat transfer between the two layers. At high Richardson number (=ratio between buoyancy and inertial force), the temperature gradient and a turbulent heat flux are not always related, but even a turbulent heat flux of a counter gradient diffusion type appears in the downstream region. Kobayashi et al. (1990, 1991) reported a mechanism of counter-gradient diffusion. They classified turbulent heat flux ($v't'$) on $u'-v'$ planes, and concluded that the turbulent lumps of higher temperature fluid move into the lower layer of lower temperature and then return to the upper layer due to a buoyancy force. However, a relationship between the counter-gradient diffusion and the large-scale coherent structure, which requires spatio-temporal information of the flow field, has never been discussed. A purpose of this works is to study the spatio-temporal heat and momentum transport in a thermal-stratified pipe flow. We experimentally measured instantaneous velocity and temperature distributions and their temporal variations by an image processing technique.

In order to obtain two-dimensional velocity distributions, several techniques were considered. Particle Image Velocimetry (PIV) and Laser Speckle Velocimetry (LSV)

are based on the pulsed laser photography of many particles undergoing short displacements. They have the advantage of high resolution in time and space (Adrian 1986). The use of optical-mechanical techniques, however, cause difficulty for time-dependent measurement of velocity fields. Recording particle images on video-recorders is expected to overcome the difficulty of PIV and to still provide enough data for statistical quantities. By a cross-correlation technique in analyzing image data, one can realize a measurement of time dependent velocity fields. It has a much simpler measuring procedure than other conventional techniques, e.g. particle tracking velocimetry which traces individual particle, and can yield velocity maps in a higher density tracer (Sakakibara et al. 1992, Yano 1983).

Planar Laser Induced Fluorescence (LIF) is attractive for measuring passive scalar such as temperature or concentration. It is non-intrusive, instantaneous and can yield information in a planar form. This technique was successfully applied to the shear layer in detecting mixing surface (Jimenez et al. 1985), concentration of two species in a turbulent flow (Komori et al. 1989) and temperature in flames (Joklik et al. 1991). In water, the temperature is evaluated from the fluorescence radiation intensity depending on the temperature. The velocity and temperature measurements using LDV has been made also employing LIF by Nakajima et al. (1990).

In the present work, a technique of time-dependent measurements of the two-dimensional velocity and temperature field was developed. Images were taken with two conventional CCD cameras, recorded on VTRs, and digitized by a digital image grabber for further data processing on the computer. Instantaneous and successive temperature and velocity maps in X-Y plane were obtained utilizing LIF for temperature and a cross-correlation technique for velocity. Subsequently, instantaneous and temporal variation of vorticity, Reynolds stress and heat flux vector distributions were evaluated from these maps. The spatio-temporal evolution of the turbulent structure were then investigated.

2 Experiments

2.1 Temperature measurement

The Laser Induced Fluorescence (LIF) was used for the measurement of concentration in a turbulent flow field with chemical reaction, where the fluorescence intensity was dependent on the concentration (Komori et al. 1989, Walker 1987 etc.). The fluorescence intensity also depends on the temperature. The fluorescence intensity (I) can be described by the following equation:

$$I = I_0 A \phi \varepsilon L C \tag{1}$$

where I_0 is the intensity of excitation beam, C is the concentration of fluorescence, ε is the molar absorptivity,

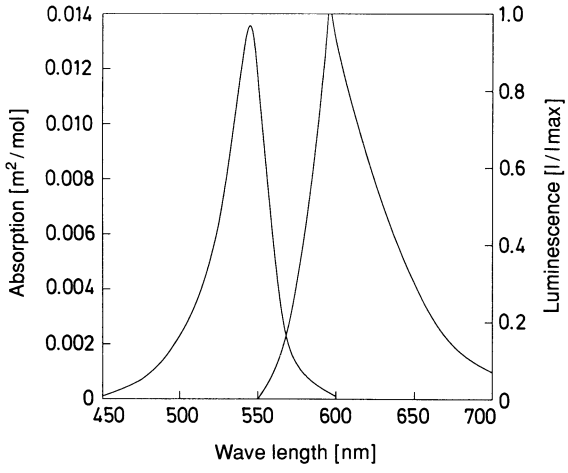

Fig. 1. Absorption and radiation spectra of Rhodamine B

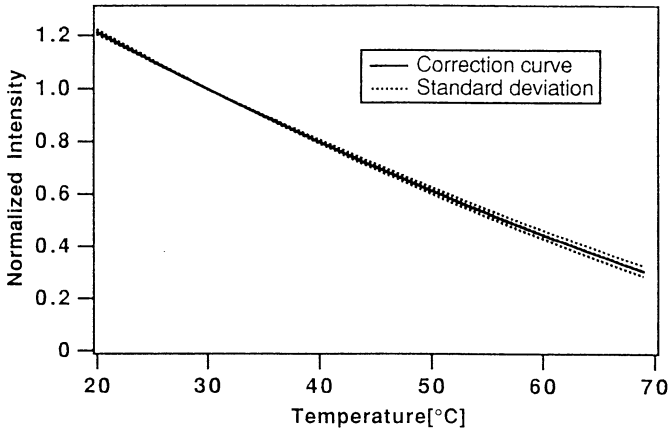

Fig. 2. Relation between the fluorescence intensity and temperature

ϕ is the quantum yield, A is the fraction of the available light collected, and L is the sampling length along the incident beam. When the concentration and the absorptivity are constant, the fluorescence intensity has negative correlation with temperature. The fluorescence intensity becomes lower as increasing temperature of the fluorescence dye. The fluorescence used in the present experiment was Rhodamine B which absorbs green light and emits orange light as shown in Fig. 1, and its intensity varies with temperature, by about 2%/K at 300 K. Oxygen molecules or metal ions act as a contaminant and decrease the intensity of fluorescence as reported by Guilbault (1973). The intensity also decreases exponentially with the lapse of time after preparation. In order to avoid these effect the experiments were carried out using boiled water prepared one day before experimentation.

Figure 2 indicates the relation between temperature and fluorescence intensity of Rhodamine B. The calibration

curve was obtained from the following procedure. The Ar-Ion laser beam was expanded by a cylindrical lens and exited the Rhodamine B solution contained in a grass vessel on a Peltier device which varied the temperature. The CCD camera faces the illuminated (by the laser) part of the fluorescence in the grass vessel. The signal from the CCD camera (SONY XC-77RR) was stored in the computer's memory via an image grabber. The temperature of the solution was measured by a C-C thermocouple and the excitation beam power was monitored by a photodetector which additionally corrected any fluctuation of the laser power. This information was recorded on a personal computer. The temperature of the solution was varied from approximately 290 K to 340 K, and the detected radiation intensity was normalized by the intensity at 303 K. A calibration curve between temperature and fluorescence intensity I_c was approximated by a second-order least-square method, based on more than 70 measurements for several concentrations of the solution ($0.1 \sim 1$ mg/l) and several excitation beam intensities. The dotted line in the figure shows the standard deviation.

The ratio between the measured intensity I and reference intensity I_{ref} of known temperature T_{ref} shows the relative intensity of the fluorescence depending on the temperature. The temperature field was computed by following equations.

$$T(x, y) = T_c\left(I_c(T_{ref})\frac{I(x, y)}{I_{ref}(x, y)}\right) \tag{2}$$

where T_c is an inverse function I_c. A distribution of I_{ref} was recorded together with T_{ref} measured by a thermo-couple under the iso-thermal condition.

The local pixel value were estimated from an averaged intensity of several pixels of the CCD camera. Since non-linearity between the input and output of the CCD camera is significant at lower light intensities, the measured intensity was compensated by using a calibration curve accounting for the non-linearity.

2.2 *Velocity measurement*

The cross-correlation technique was employed to obtain the velocity vectors for each location. Figure 3 graphically shows the principle of the method. The small area at $t = t_n$, the reference matrix, was searched over an interrogation window at $t = t_n + \Delta t$. The corresponding matrix was identified by the maximum coefficient of the cross-correlation between the reference matrix and the small area in interrogation window. The velocaity vector was evaluated from the displacement and time interval (Δt) between the reference matrix and the corresponding matrix. The initial size of the correlated area was variable, so that the best size for this pattern area might be dictated by the density of the tracer particles and local strain rate in a flow. When the density of particles was not enough, the reference matrix contained little valid information and the number of erroneous vectors increased due to the difficulty of finding the maximum correlation coefficient. At minimum, the reference matrix had to have at least 3–4 particles in it. The technique assumed that the image of the local flow pattern is not substantially differ from that of the previous picture, i.e., the number of erroneous vectors increased with an increase in strain rates (Yamamoto et al. 1989). The actual size of the reference matrix will be discussed in Sect. 2.5.

There are some cases where the correlation value of another vector exceeds that of the correct vector. To estimate the correct vectors, a verification procedure was established. As a first step, the vectors are calculated over the entire plane while memorizing the second and third highest correlation values and it's displacements. A result with erroneous vectors is caused by wrong particle pairing. If a vector is considerably different from the average

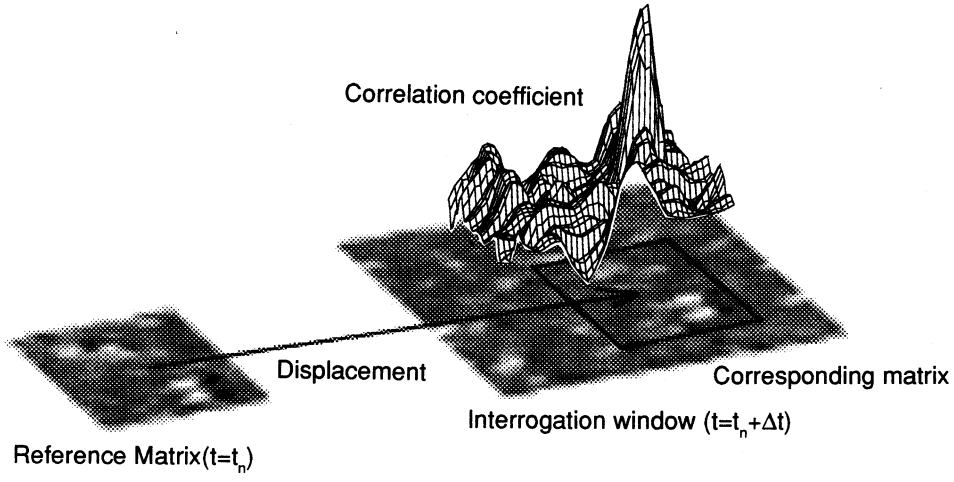

Fig. 3. Schematic of the correlation technique

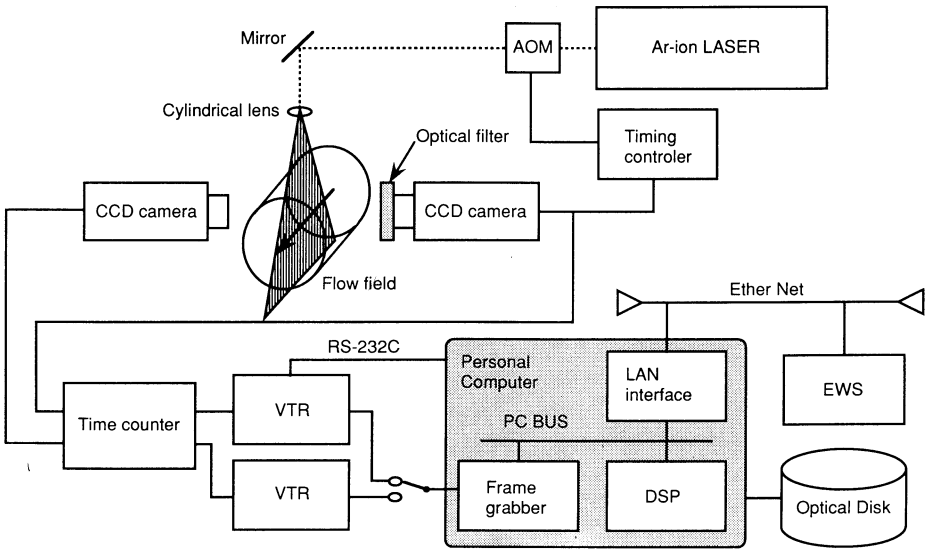

Fig. 4. Hardware setup

vector calculated from the surrounding vectors, the most similar vector was chosen out of the second and the third vector. In the present study the verification procedure was repeated 5–6 times and found sufficient as did Landreth & Adrian (1988). After the procedure, however, still remained some unacceptable vectors. These vectors are recalculated changing the size of reference matrix from 5×5 to 30×30 pixels. If a more preferable vector is obtained in this re-calculations, it is replaced the previous vector. The re-calculation procedure was repeated 2 times.

2.3 System setup

Figure 4 illustrates the system set-up. The flow was marked with tracer particles for velocity and with the fluorescence dye, Rhodamine B, for temperature measurements. A plane which was normal to the spanwise direction in the pipe was illuminated by a laser sheet (4 W Ar-Ion laser, INNOVA 70). The pulse width and time interval of the laser sheet are controlled synchronously with two CCD cameras (XC-77RR, NTSC 768×493 pixel, SONY) which view the same measuring region simultaneously. To generate the synchronized stroboscopic illumination, an acoustic optical modulator (AOM) cell (Model A-160, HOYA) chopped the laser beam. The AOM was synchronized with the vertical signal of the CCD cameras. Video signals from the CCD cameras were recorded on separate VTRs (AG-5700, S-VHS, Panasonic). A simple scheme to tag the image frames was developed to identify the individual planes; a bar-code field number was superimposed on the left side of each video field. The bar-code consisted of a 24 bits binary, where one bit was 8 by 8 pixels square colored black or white corresponding respectively to 0 and 1. This bar-coded number was incremented with the CCD vertical

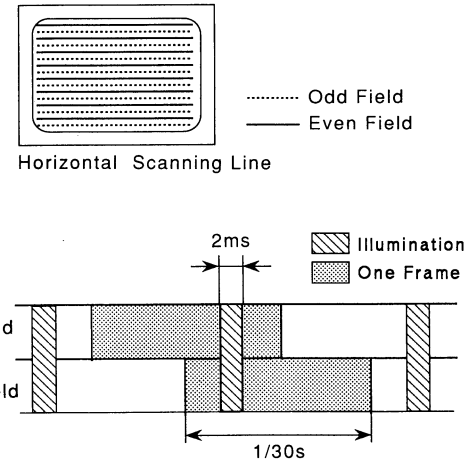

Fig. 5. Illumination timing of the laser sheet

signals at the start of every video field. The laser sheet was synchronized with the even numbers of the bar-code and illuminated a single pulse in one video frame. This technqiue allowed one to take the same image for both the odd and even fields as shown in Fig. 5.

To capture the expected planes after recording, the image grabber (512×512 pixels, 8 bit, 4 planes) continuously overwrote the images from the VTR to the video memory, and the personal computer simultaneously read the bar-code number from the video memory. When the field number coincided with the expected field number, the image grabber stopped writing and held the image in the video memory. From these images, the temperature distribution and the velocity vectors were evaluated using LIF and the cross-correlation technique by employing a DSP (Digital Signal Processor, Texas Inst., TMS320C30)

which was installed in the personal computer. With the smaller computer system used in the laboratory, the processing procedure should be accelerated to obtain the velocity and temperature as soon as possible while conducting the experiments. Sequential handling and the calculation used in processing was accelerated by the DSP. The personal computer transported the reference matrix and interrogation matrix from video memory to the DSP local memory. The DSP computed the correlation coefficients simultaneously with the data transfer. After the corresponding matrix displacement positions were calculated, the velocity was computed from the displacement distance (Maeda et al. 1992). The temperature was evaluated from intensity distribution of the fluorescence images. These results were stored onto a magnetic optical disk (MO Disk). The sequence of capturing the expected images and the image processing was performed automatically and continuously without human iterration. The time-dependent 2-D velocity and temperature dataset accumulated in the computer stage was transferred to an engineering work station (EWS) via Ethernet, and the mean values, fluctuations, correlations, and other statistical values were therein calculated.

2.4 Comparison between image processing and point measurement

Laser Doppler Velocimetry was also used simultaneously to measure velocity of the flow for verifying the results of this measuring system. The image processing results were presented for the thermally stratified pipe flow at the point 5 mm upstream from an LDV measurement point, avoiding the interference by illumination of LDV beams. Figure 6a shows the time-series streamwise velocity fluctuations simultaneously measured by the present system and LDV. Both results has a good agreement to reveal the large scale motion of the fluid. Higher frequency velocity fluctuations were not obtained by the present image processing as measured by the LDV system. This result would be caused by the difference of the time resolution between LDV and image processing. Measurements by LDV indicates the instantaneous velocity every 1/30th of a second, while the image processing gives the time-averaged velocity within the interval of 1/30 s. The temperature measurement compared with a point data by a thermocouple is also in good agreement and confirmed reliable results for the evaluation of fluctuation as shown in Fig. 6b.

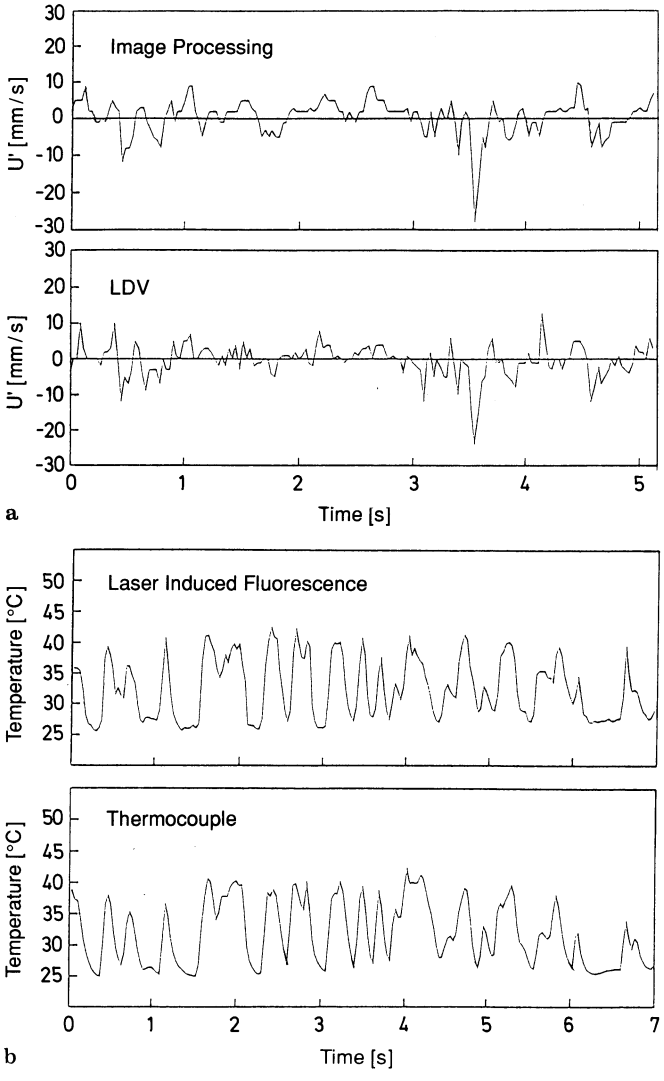

Fig. 6a and b. Comparison of the results between the image processing and the point-measurements; **a** Correlation technique and LDV; **b** LIF and thermocouple

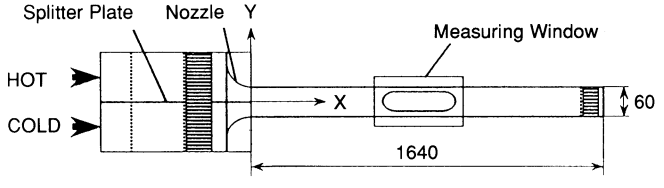

Fig. 7. Flow system and coordinates

2.5 Flow configuration

The experimental apparatus is schematically illustrated in Fig. 7. The test section of constant diameter $D=60$ mm and a total length of 1640 mm is set horizontally. The higher temperature water at lower velocity flows into the upper settling chamber, and the lower temperature water at high velocity flows into the lower chamber. Both flows pass through the nozzle and form an uniform velocity and temperature distributions at the end of the splitter plate. It was then led to the measurement region which was located at a fixed position $X/D=12$. Cartesian coordinates were adopted with the origin fixed at the trailing

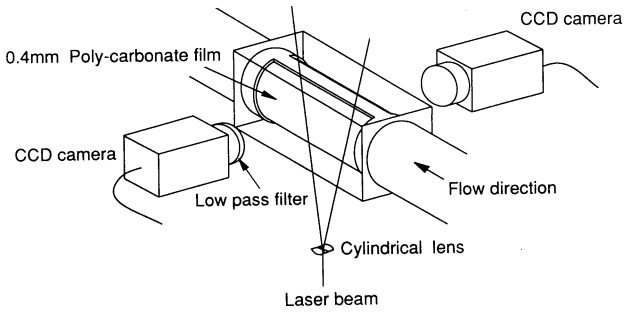

Fig. 8. Test section and camera arrangement

edge of the splitter plate. In the experiments, the bulk Reynolds number $Re_b = U_b D/\nu$ was set at 7400, where U_b denotes a bulk velocity, ν denotes the kinematic viscosity evaluated at a temperature corresponding to the flow in the lower half. The velocity of upper and lower stream U_2, U_1 were 100 mm/s and 140 mm/s, respectively. Under stratified condition, the temperature of the flow in the lower half T_1 was 294 [K], and the temperature difference between hot and cold streams ΔT was 22 K. The overall Richardson number $Ri = \beta g D \Delta T / \Delta U^2$ is 2.5, where $\Delta U = U_1 - U_2$. Polystyrene particles of 5 μm mean diameter were used as the tracer particle, and 0.5 mg/l fluorescence dye (Rhodamine B) was mixed in the solution.

In order to eliminate the reflection from the laser light sheet at the surface of the circular pipe, a measuring window was specially designed; a slit was machined along the measurement width of the pipe and coated there with a thin poly-carbonate film whose thickness was 0.4 mm. This slit with the thin film was enclosed in an acrylic duct filled with water as illustrated in Fig. 8.

Two CCD cameras faced each other across the pipe, and faced the same plane which was illuminated by a laser sheet projected from the lower side of the pipe. To find the correspondence between actual length and pixel length in the images, parallel beams of the He–Ne laser with a width of 25.0 mm was put in the measuring plane and the pixel width of two beams in a image was measured on the image grabber. In the present experiment, 126 pixels corresponded to 10 mm for the particle image, 129 pixels to 10 mm for the fluorescence image. The correspondence between actual position and pixel position was also determined by cross beams with the same laser inserted in the measuring region. These operations enabled a complete matching between both planes of velocity and temperature. The size of reference matrix in particle image was 28×28 square pixels, and the avaraging area of the fluorescence image was 8×8 square pixels. The time interval between the reference image and the target image (Δt), and that between the successive velocity and temperature field was 1/30th of a second, respectively. One thousand velocity and temperature maps under isothermal and stratified condition were obtained respectively.

3 Results and discussion

3.1 Time-averaged velocity and temperature profile

Figure 9 shows a time-averaged streamwise velocity, and turbulent intensities at the location $X/D = 12.3$. A temperature profile at the same location is given in Fig. 10. At this measured position, the mixing layer is fully developed and it is known that its thickness is constant in this region of a stratified pipe flow (Kobayashi et al. 1990). The local

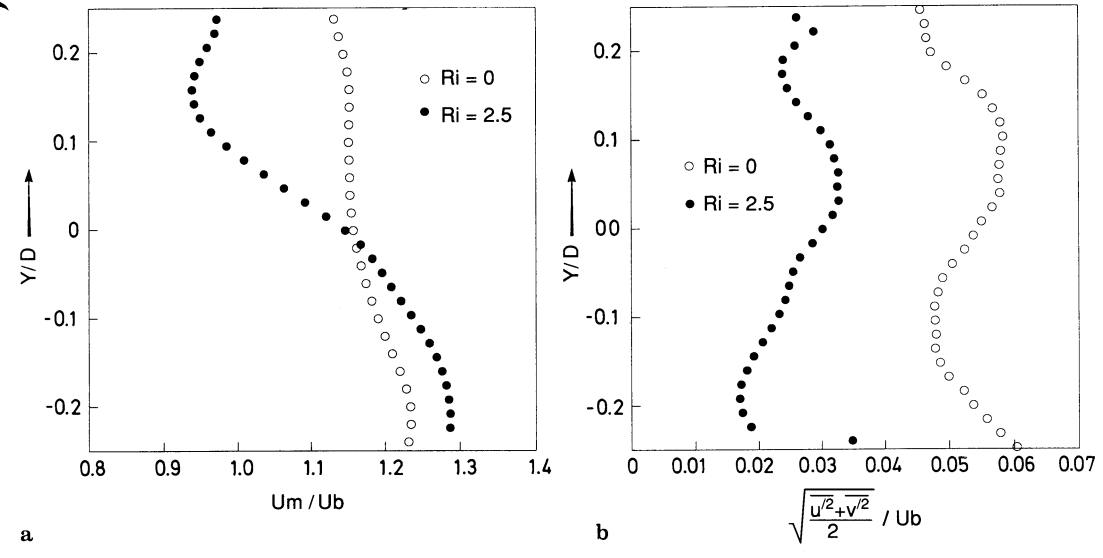

Fig. 9. a Distribution of time-averaged streamwise velocity at $X/D = 12.3$; **b** distribution of turbulent intensities at $X/D = 12.3$

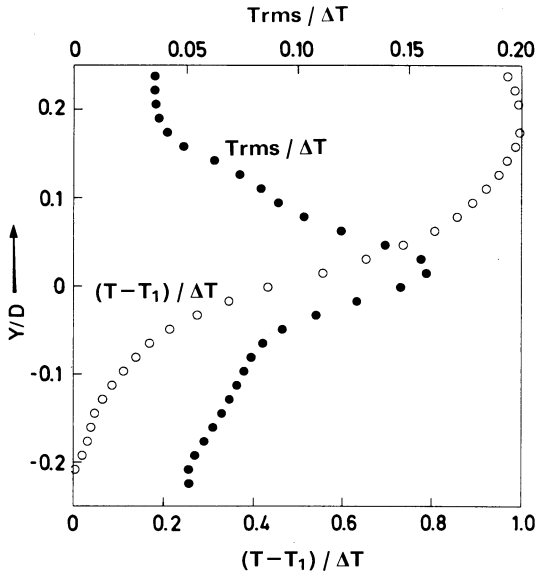

Fig. 10. Distribution of time-averaged temperature and its turbulent intensities at $X/D=12.3$

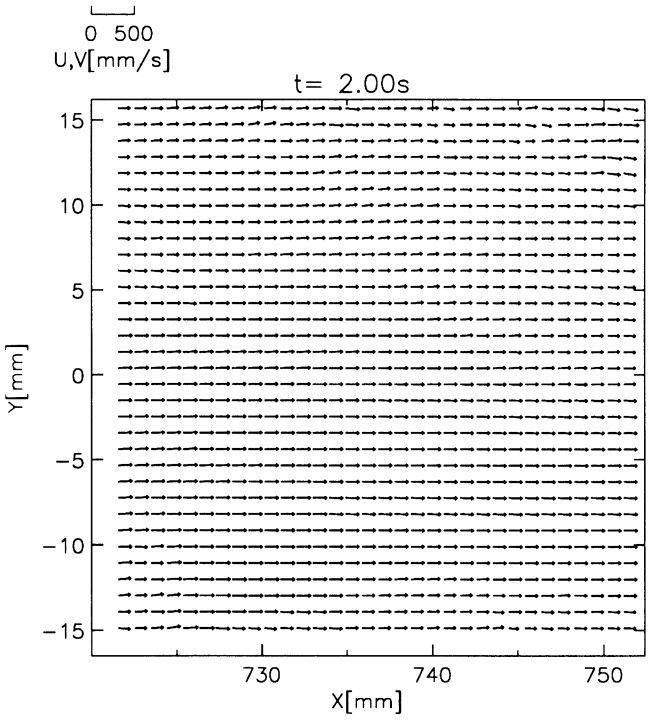

Fig. 11. Instantaneous velocity map under isothermal condition ($Ri=0$) with dimensional size and range of velocity

velocity and temperature are normalized by the bulk velocity (U_b) and temperature difference between upper and lower layers (ΔT). The velocity gradient at the center of the pipe is larger for $Ri=2.5$ than for $Ri=0$. The minimum velocity is observed in the velocity profile and it is located at $Y/D=0.13$ for $Ri=2.5$ where a strong stratification exists. This is caused by the existence of the minimum velocity in the inlet velocity distributions (Kobayashi et al. 1990). The turbulent intensity also becomes smaller for $Ri=2.5$ than for the isothermal condition, $Ri=0$, because the buoyancy force suppresses the mixing. These results are in a qualitative agreement with characteristics measured by LDV and thermocouple (Kobayashi et al. 1990).

3.2 Instantaneous velocity, vorticity and temperature maps

Figure 11 shows an instantaneous velocity map ($U(X, Y, 0, t)$, $V(X, Y, 0, t)$) under isothermal condition. The position and velocity vectors are dimensional in order to show the actual size of the measured region and velocity range. As the convection velocity is far larger than the fluctuating velocity, all vectors have almost the same length and direction, so that it is difficult to recognize the difference between each vectors in the figure. For a better presentation, the constant velocity U_c, which is a time-averaged streamwise velocity at $Y/D=0$, was subtracted from the streamwise velocity component U. Figure 12a shows the resulting velocity vector map ($(U(X, Y, 0, t) - U_c)/U_b$, $V(X, Y, 0, t)/U_b$). The flow structures are represented more clearly. The velocity vectors are non-dimensionalized by the bulk velocity U_b. Figures 12b and c are successive maps with a 2/30th seconds time interval after Fig. 12a. In these figures, the spanwise vorticity maps are superposed in gray-scale. Spanwise vorticity was computed from circulation to eliminate an error caused by differencing as follows,

$$\omega=\frac{\Gamma}{A}=\frac{\int_A\left(\frac{\partial v}{\partial x}-\frac{\partial u}{\partial y}\right)dA}{A}=\frac{\oint_S(udx+vdy)}{A}$$

where A is the area of a region surrounded by S. In the present case, A is 7.3 mm^2 in an actual plane.

In Fig. 12a, a long vortex of positive vorticity (marked by (1) in the figure) is observed, which extends from $X/D=12.15$, $Y/D=0.2$ to $X/D=12.50$, $Y/D=0.03$. Convecting feature of this flow pattern can obviously be observed from a time change of velocity maps. In Fig. 12b, the vortex (1) is convected downstream, and the tail of the vortex is observed at $X/D=12.4$. The other vortex (2), which extends from $X/D=12.0$, $Y/D=0.05$ to $X/D=12.35$, $Y/D=0.15$, appears from the upper stream. In Fig. 12c, the vortex (1) disappear downstream. Downward and slower velocity vectors (4) are observed in the upper layer, and upward and faster velocity vectors (3) are observed in the lower layer. The vortex (2) is induced by these upper and lower stream (3) (4).

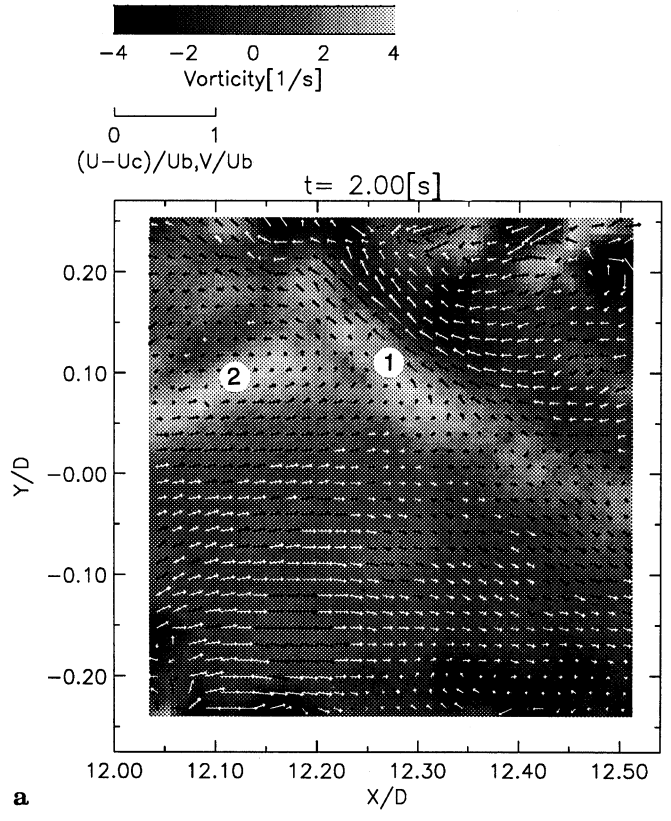

a

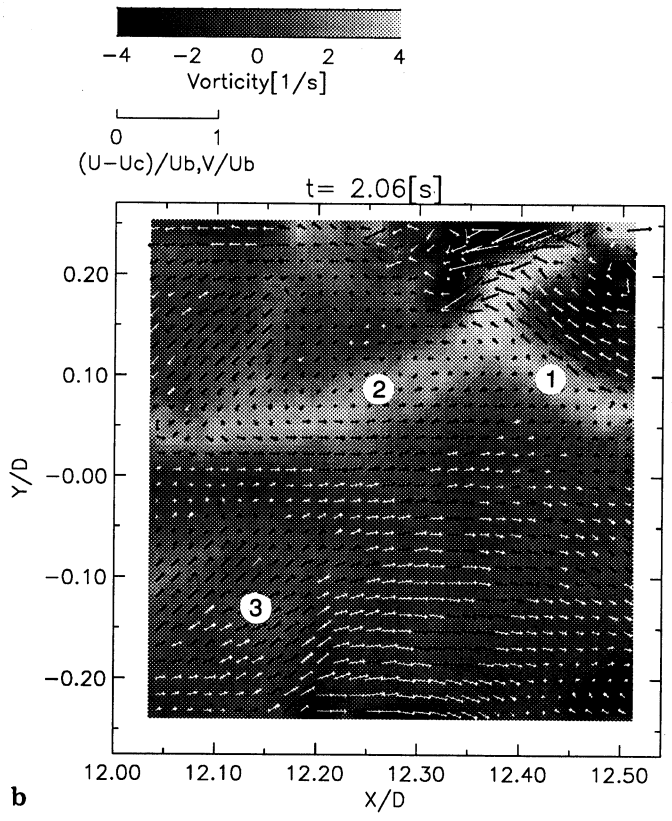

b

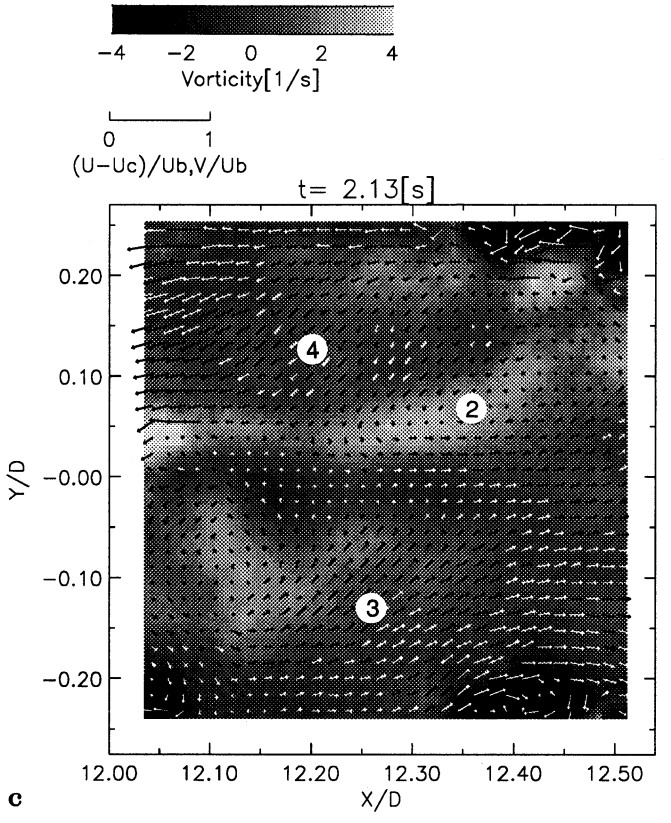

c

Fig. 12a–c. Successive velocity and vorticity maps with 0.033 seconds time interval under isothermal condition ($Ri=0$)

Figure 13 shows successive maps of instantaneous temperature distributions with a time interval of 2/30th seconds under stratified condition. Simultaneous velocity map is overlaid for each temperature distribution. The color scale denotes the temperature T^* normalized by the temperature difference ΔT. Generally in these figure (a) to (c), the velocity is lower and temperature is higher in the upper layer than in the lower layer. In Fig. 13a–c, a lump of $T^* = 0.7 \sim 0.8$ (yellow, marked by 5), is elongated into a part of $T^* = 1.0$ (red) at $Y/D = 0.08$ from right to left. We call this a 'crest'. Similarly (but in the lower layer), a part of $T^* = 0.1 \sim 0.2$ (blue, marked by 6), is entrained into a part of $T^* = 0$ at $X/D = 12.3$ from left to right. We call this a 'valley'. The elongation of the 'crest' and 'valley' are most likely by a roll-up motion of fluid induced by the mean shear. This flow structure is convected to downstream, Fig. 13a–c.

Corresponding vorticity maps are presented in Fig. 14a–c. Figure 14a shows two elongated vortices, one (7) extending over the 'crest' and the other (8) from the left and beneath the 'crest'. It shows a strong inclination on the right of the area of view. After 2/30th seconds (Fig. 14b) the vortex (7) moves downstream, and the vortex (8) lies along a boundary of $T^* = 0.7$ and 0.9 (yellow and red), with an included part having been connected and disappeared out of the area of view. The subsequent inclined vortex (9) which appears from the left side of the area of view, in Fig. 14b, extends along the left side slope of the 'valley'. In Fig. 14c, the vortex (7) has almost disappeared, the vortex (8) and (9) are connected together at the left side. This sequence will be discussed in the next section.

3.3 Temporal variation of velocity, vorticity and temperature

In order to see a temporal variation of the temperature and velocity fields, vertical distributions of velocity, vorticity and temperature profiles at $X/D = 12.3$ are plotted on the Y-t plane using a color scale (Figs. 15–17). The time coordinate can be approximately converted to a streamwise distance by the relation $X = -U_c t$. Each figure does not necessarily display the flow along the test section. However, it can be expected that a picture of this sort for a short period of time and short span of space can be displayed in this form of representation.

Figure 15 is a vorticity variation for isothermal condition ($Ri = 0$). The vorticity value is presented by the color scale. Simultaneous velocity vectors are superposed on this figure. The vortices of positive vorticity appear irregularly, most of which are short. Some other long ones, however, are roughly parallel, extending over the whole height between the top and bottom. The vortices in Fig. 12 are observed at $t = 2.0 - 2.3$ (marked by 1, 2).

Figure 16, for a stratified condition ($Ri = 2.5$) shows a significant difference on the appearance of vortices of positive vorticity. The vorticity and velocity scales are same as that of Fig. 15. Temporally, it looks more periodical. On the figure, these vortices start in the upper layer, roughly at $Y/D \sim 0.15$ and extends near to $Y/D \sim -0.2$. Spatial extension and inclination of vortices (7, 8, 9) in Fig. 13a–c are well understood at $t = 2.0$–2.3. Connection of these vortices are observed at $Y/D = 0$ to 0.1 and the vortices of high vorticity (red) can be seen at this region.

The time-averaged vorticity values and their RMS values are given in Figs. 18a and b for isothermal and stratified conditions. Under stratified condition ($Ri = 2.5$) the vorticity has a large peak at $Y/D = 0.05$ corresponding to a large velocity gradient, in Fig. 9. But its RMS value is smaller than for $Ri = 0$. This implies that the shedding of strong vortices are suppressed by buoyancy force, in spite of the larger velocity gradient.

The temperature variation is shown in Fig. 17. The series of 'crests' (which appears around $Y/D = 0.05$) and 'valleys' ($\sim Y/D = -0.1$) from a 'saw-tooth' pattern on the thermal interface. This temperature pattern corresponds quite well to the inclined vortices in Fig. 16. The lines marked in Fig. 16 are overwrote by 7, 8, 9. Moreover, it is consistent with the aspects discussed for instantaneous temperature and vorticity maps in Sect. 3.2. The inclined vortices are aligned by left side of the 'crest' and 'valley'. This kind of structure is characteristic of the stratification. As the buoyancy force suppresses the mixing, the mean velocity gradient becomes steeper and results in the stronger shear rate at the thermal interface. This produces the inclined positive vortices.

3.4 Temporal variation of Reynolds shear stress

Temporal variation of the instantaneous Reynolds shear stress are given in Figs. 19 and 20 corresponding to the isothermal and the stratified conditions respectively. For the isothermal condition, strong positive and negative Reynolds stress appears irregularly over the measured region. The width of these region is roughly 0.1–0.2 D. The absolute value of the Reynolds stress is relatively small under stratified conditions and the width is also smaller than that under isothermal conditions. The appearance of the high Reynolds stress region is less frequentry. High Reynolds stress regions can be observed above the 'crest'. The momentum is mainly transported by large coherent structure like 'crest' and 'valley' under stratified condition.

3.5 Instantaneous turbulent heat flux vector maps and its temporal variations

For understanding the transport of heat, distributions of turbulent heat flux vectors ($u'T'$, $v'T'$) are shown in Fig. 21 with the overlaid temperature map of Fig. 13b. The downward heat flux vectors (co-gradient type, marked by 10) are concentrated just above and below the centerline. It is

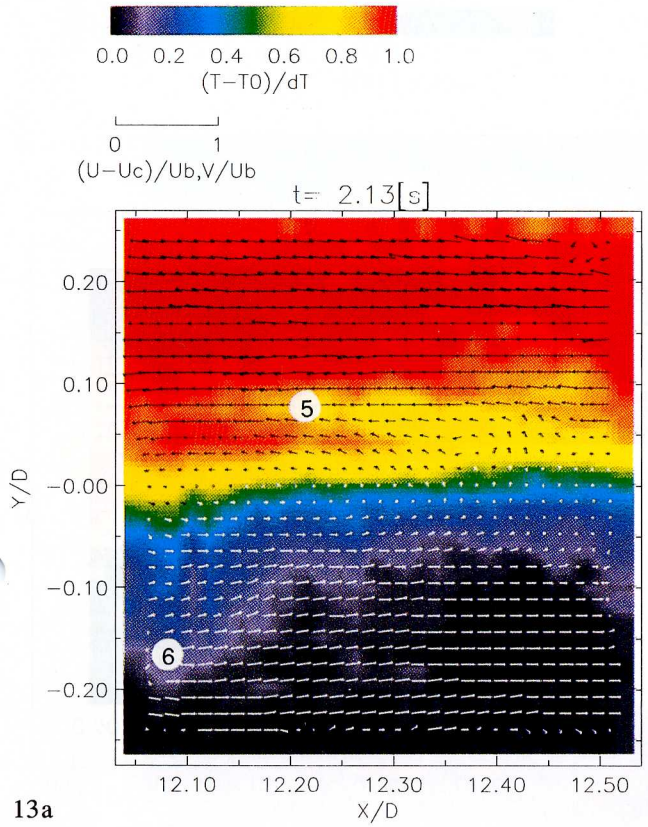

13a

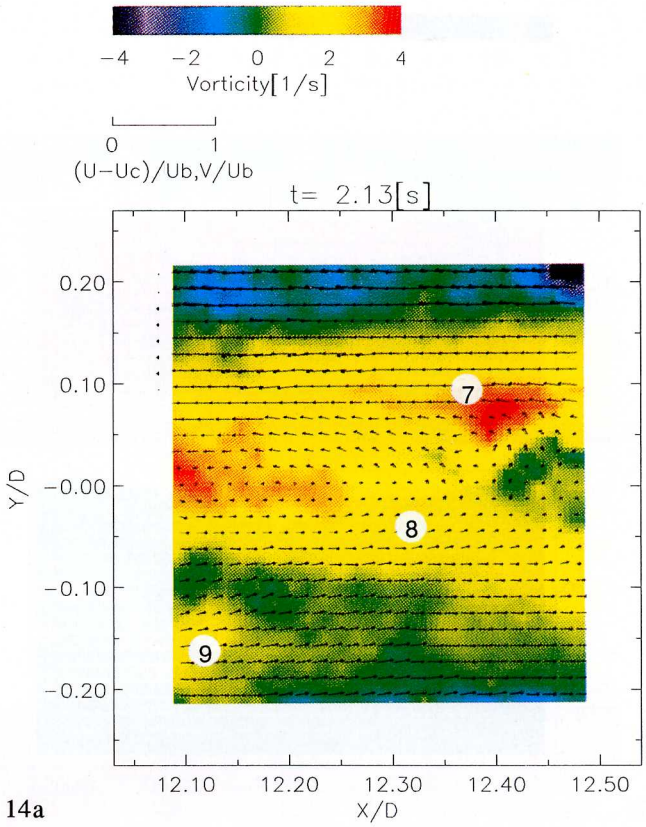

14a

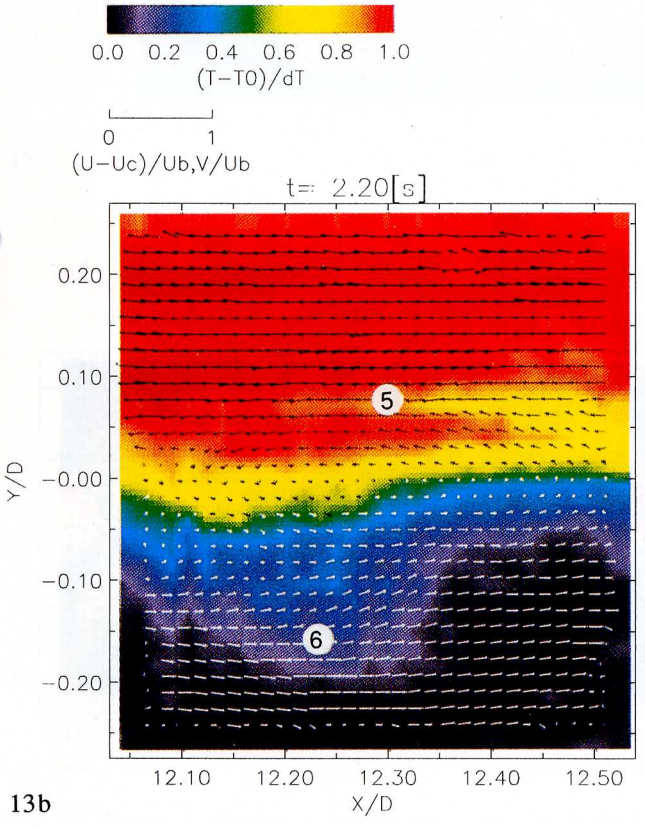

13b

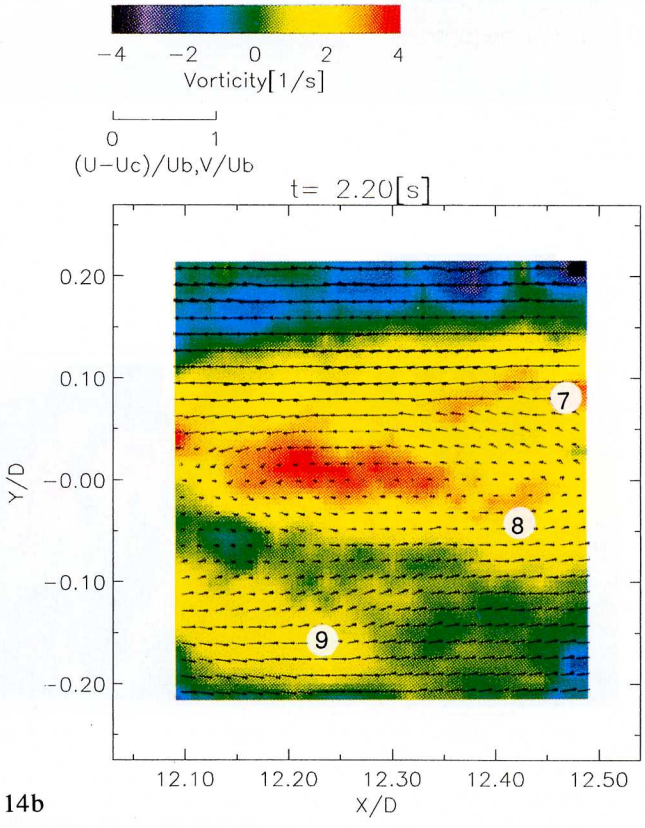

14b

Fig. 13a, b

Fig. 14a, b

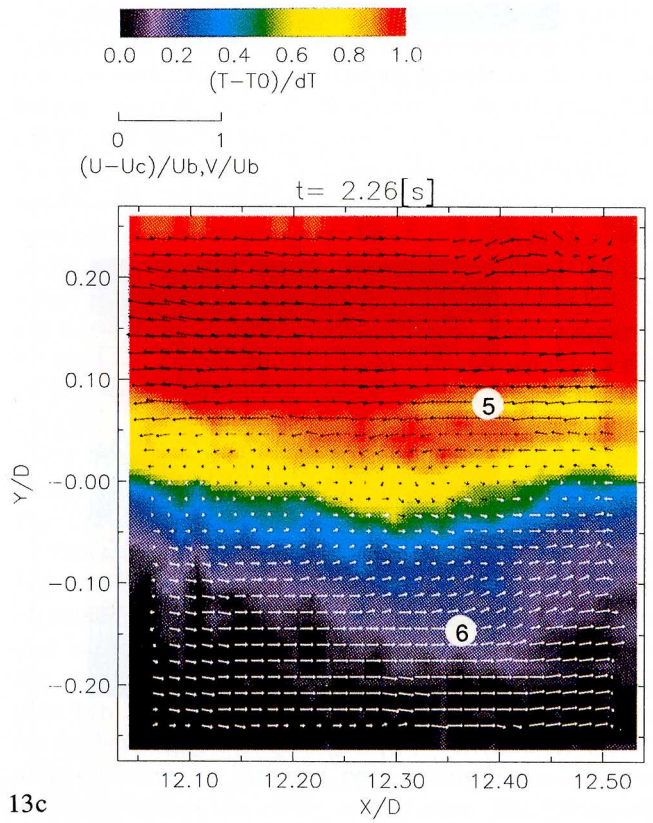

13c

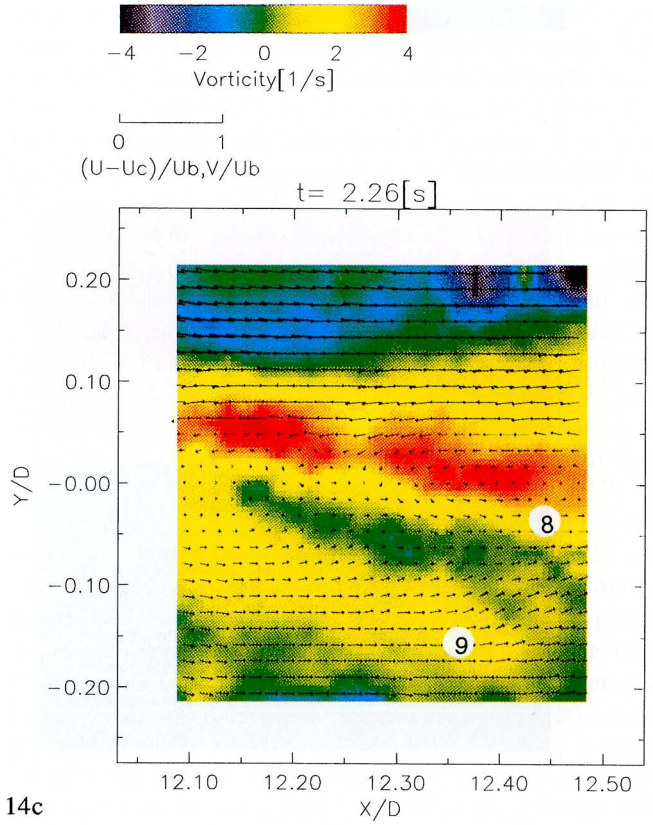

14c

Fig. 13a–c. Successive velocity and temperature maps with 0.066 s time interval under stratified condition ($Ri=2.5$)

Fig. 14a–c. Successive vorticity maps corresponding to Fig. 13

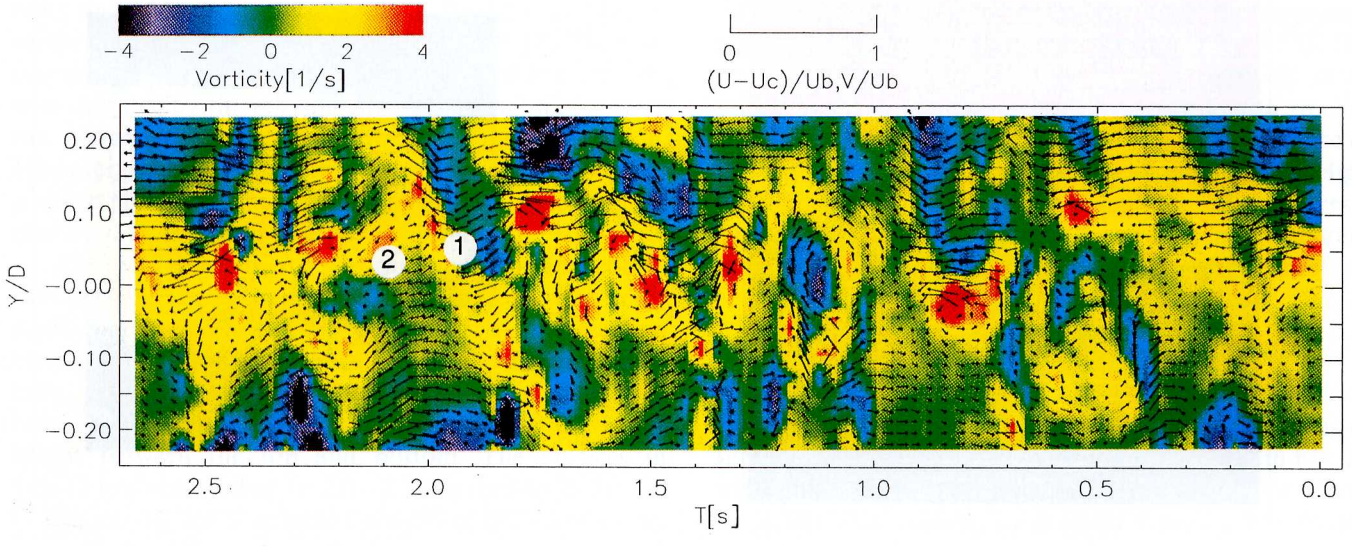

Fig. 15. Temporal variation of velocity and vorticity at $X/D=12.3$ under isothermal condition ($Ri=0$)

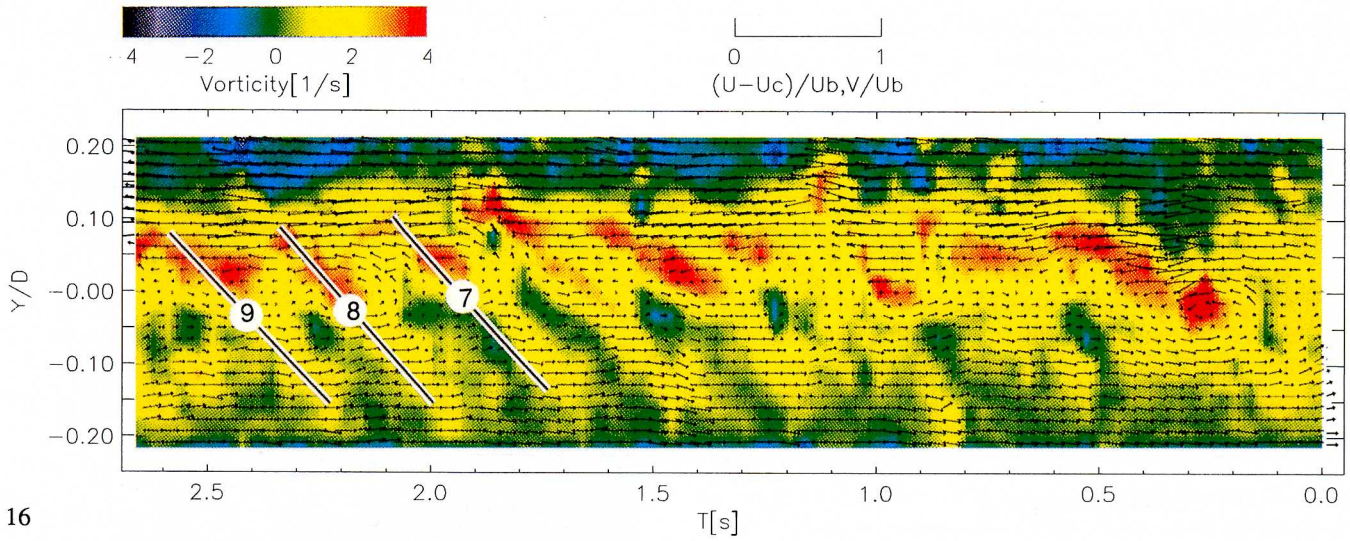

16

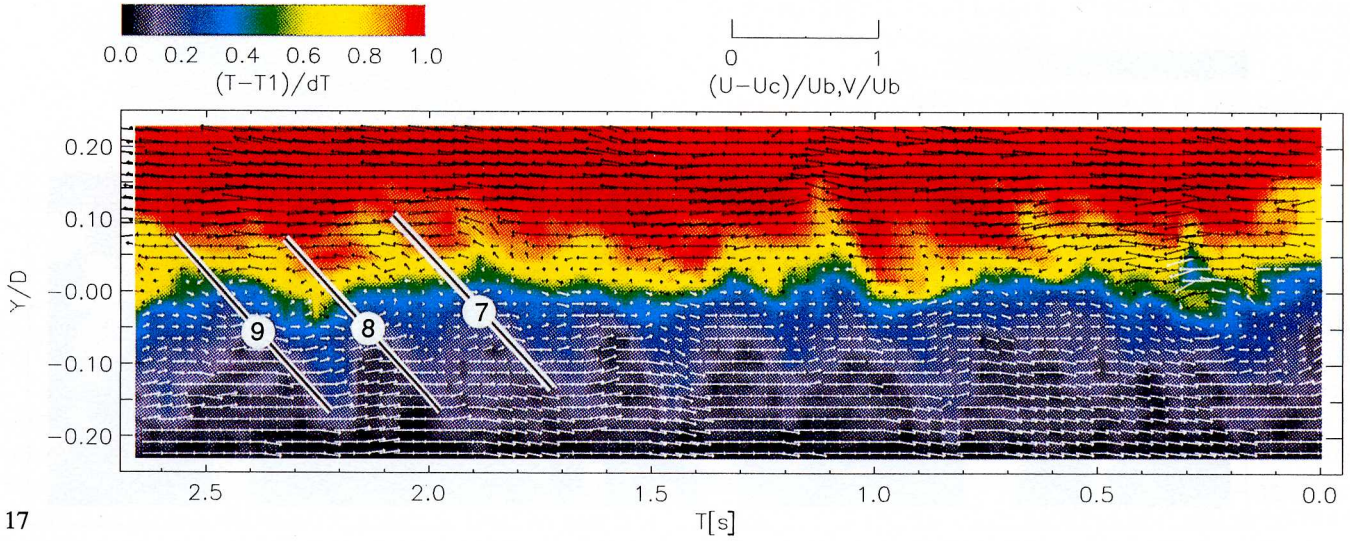

17

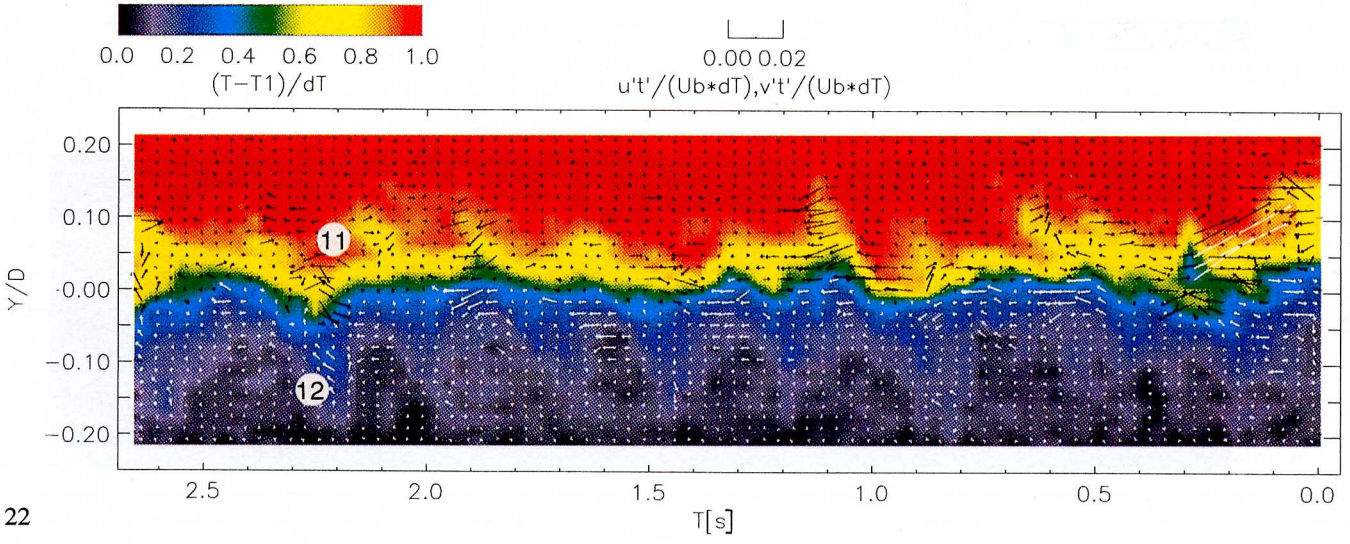

22

Fig. 16. Temporal variation of velocity and vorticity at $X/D=12.3$ under stratified condition ($Ri=2.5$)
Fig. 17. Temporal variation of temperature at $X/D=12.3$ under stratified condition ($Ri=2.5$)
Fig. 22. Temporal variation of heat flux vector ($u'T', v'T'$) under stratified condition ($Ri=2.5$)

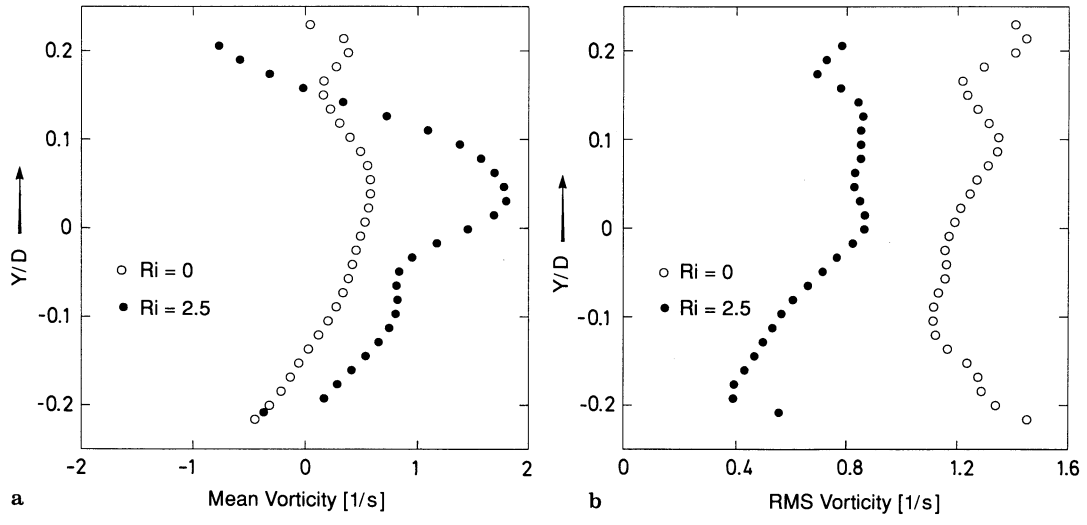

Fig. 18

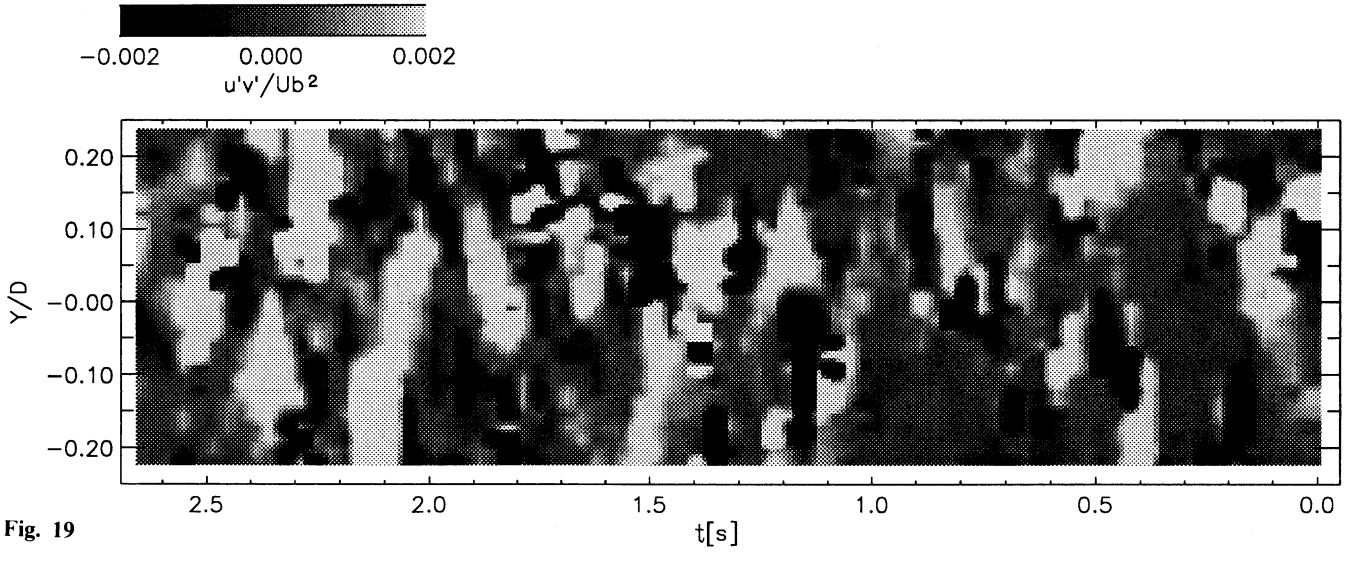

Fig. 19

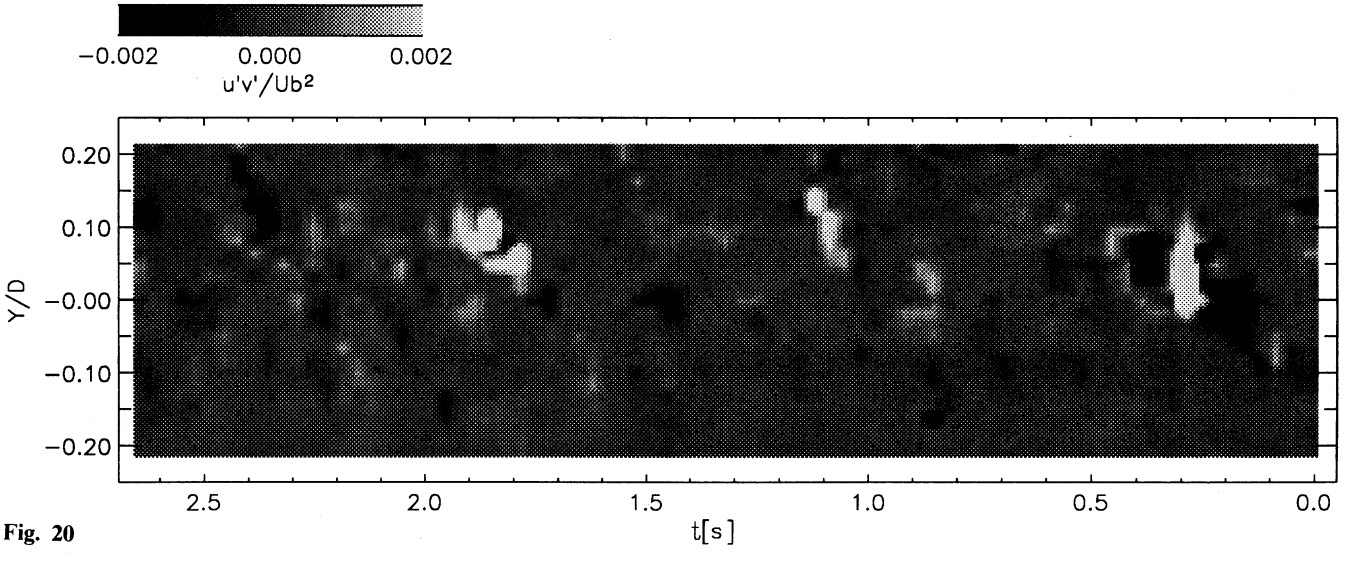

Fig. 20

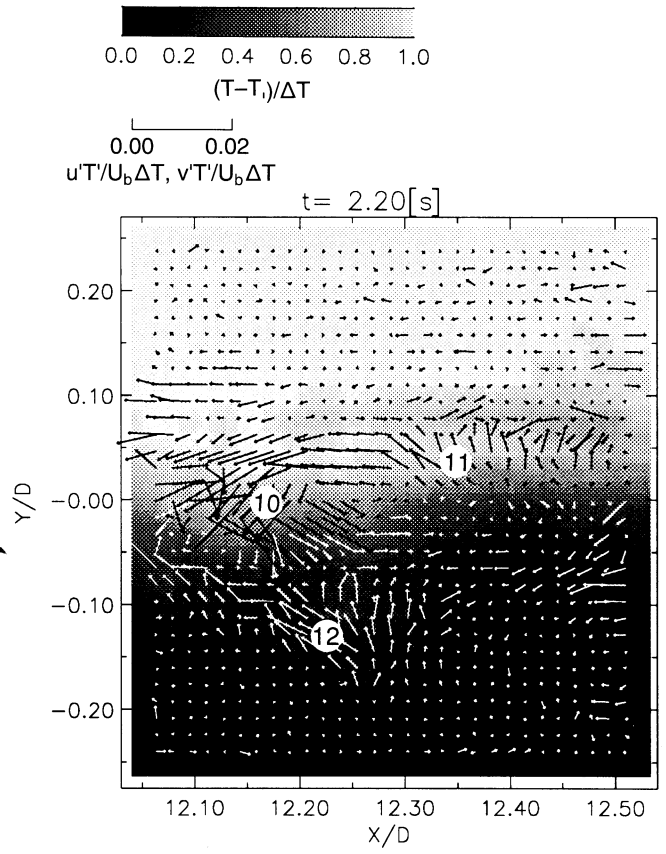

Fig. 21. Instantaneous heat vector map corresponding to Fig. 14b, overlaid with a temperature map

observed that the 'crest' and 'valley' are associated with upward heat flux vectors (counter-gradient type, 11, 12). Figure 22 shows the temporal variation of the heat flux vector. Occurrence of the larger values of absolute heat flux is roughly coincident with that of the 'crest' and 'valley'.

It is considered that the strong heat exchange and momentum transfer occurs near the 'crest' and 'valley'. If the 'crest' and 'valley' flow up away from centerline by roll-up motion induced by mean shear, co-gradient type momentum and heat transport would become dominant. The counter-gradient type diffusion would occur, when the 'crest' and 'valley' return to the centerline due to a inertial motion and presumably buoyancy forces.

At the location where the counter-gradient diffusion occurs (Kobayashi et al. 1990), the return motion of the 'crest' and 'valley' may be more dominant than that moving away from the centerline. This unbalanced flux of heat and momentum might be caused by the existence of a long internal wave in the pipe.

Fig. 18a and b. Distributions of time-averaged vorticity (**a**) and its RMS value (**b**)
Fig. 19. Temporal variations of Reynolds shear stress at $X/D = 12.3$ under isothermal condition
Fig. 20. Temporal variations of Reynolds shear stress at $X/D = 12.3$ under stratified condition

4 Conclusion

Two-dimensional time-dependent velocity and temperature fields of a stable thermally stratified pipe flow was measured by using an image processing technique (correlation technique and LIF) to capture the instantaneous structure of turbulent mixing accompanied by the heat and momentum transfer. One thousand instantaneous velocity and temperature distributions were obtained successively. The vorticity, Reynolds stress and heat flux vectors were estimated.

A roll-up motion at the thermal interface was observed under stratified conditions. The colder, bulk water entering the hot layer are recognized as a 'crest' and the hot water entering the cold layer as a 'valley'. They are located above and below the centerline, and were elongated backwards and forwards respectively. The elongated and inclined vortices extend from the bottom of the 'valley' to the top of the 'crest', being attached to the 'crest' and 'valley'. They are connected together at the lower part of the 'crest'. Many of these structures were also observed in temporal variations of vorticity and temperature, which appeared more quasi-periodical than that under isothermal conditions. This structure is caused by buoyancy force. As the buoyancy force suppresses the mixing, the mean velocity gradient becomes steeper and results in the stronger shear rate at the thermal interface. This produces the inclined positive vortices.

The instantaneous distributions of the heat vectors and temporal variations of the heat vectors and Reynolds shear stress showed the strong exchange of heat and momentum occur through the 'crest' and 'valley'. Instantaneous co-gradient and counter-gradient type of diffusion of heat and momentum have been recognized in the 'crest' and 'valley'.

Acknowledgements

The authors acknowledge Dr. K. Kobayashi of the Tokyo Institute of Technology and graduate students S. Katsu and G. Kamiya of Keio University who participated in these experiments. Authors are thankful to Dr. Y. Takeda and Dr. A. Tokuhiro of the Paul Scherrer Institute in Switzerland for their helpful discussions and encouragement. Analyzing experimental data was performed at the Paul Scherrer Institute. This work was partly supported by a grant in Aid for scientific research by the Ministry of Education of Japan under Grant No. 04555050.

References

Adrian, R. J. 1986: Multi-point optical measurements of simultaneous vectors in unsteady flow – a review. Int. J. Heat & Fluid Flow 7, 127–145

Guilbault, G. G. 1973: Practical technique for measurement: theory, methods and techniques. New York, Dekker

Jimenez, J.; Cogollos, M.; Bernal, L. P. 1985: A perspective view of the plane mixing layer. J. Fluid Mech. 152, 125–143

Joklik, R. G.; Horvath, J. J.; Semerjian, H. G. 1991: Temperature measurements in flames using thermally assisted laser-induced fluorescence of Ga. Appl Opt 30: 12, 1497–1504

Kobayashi, K.; Hishida, K.; Maeda, M. 1990: Turbulent transport across stable thermal stratified layer in a circular pipe. Proc. 9th Int. Heat Transfer Conf., Jerusalem/Israel, Vol 5, pp 341–346

Kobayashi, K.; Sakakibara, J.; Hishida, K.; Maeda, M. 1991: Time-series measurements of turbulent flow field using image processing system, proceedings, experimental and numerical flow visualization 1991. Winter annual meeting ASME, Atlanta, pp 155–162

Komori, S.; Kanzaki, T.; Murakami, Y.; Ueda, H. 1989: Simultaneous measurements of instantaneous concentration of two species using mixed in a turbulent flow by using a combined laser-induced fluorescence and laser-scattering technique. Phys. Fluids A 1, 2, 349–352

Landreth, C. C.; Adrian, R. J. 1988: Impingement of a low Reynolds number turbulent circular jet onto a flat plate at normal incidence. 11th Symposium on Turbulence, Rolla, MO

Maeda, M.; Sakakibara, J.; Hishida, K. 1992: Field measurements of velocity and temperature by digital signal processing. ICHMT Int Seminar, Imaging in Transport Processes, pp 239–248

Nakajima, T.; Utsunomiya, M.; Ikeda, Y.; Matsumoto, R. 1990: Simultaneous measurement of velocity and temperature of water using LDV and fluorescence technique. 5th Int. Symp. on Appl. of LASER Tech. to Fluid Mech., Lisbon, 12.1

Sakakibara, J.; Hishida, K.; Maeda, M. 1992: Simultaneous and time series measurements of two-dimensional velocity and temperature fields using an image processing technique. 6th Int. Symp. on Appl. of LASER Tech. to Fluid Mech., Lisbon, 23.5

Walker, D. A. 1987: A fluorescence technique for measurement of concentration in mixing liquids. J. Phys. E. Sci. Instrum. 20: 217–224

Yamamoto, F.; Dai, Y.; Koukawa, M.; Itoh, M.; Uemura, T. 1989: Numerical simulation on error analysis in particle tracking velocimeter by correlation method. Proceedings, Flow Visualization-1989, Winter annual meeting ASME, California, pp 9–14

Yano, M. 1983: Velocity measurement using correlation concerning with digital tracer image, Journal of the Flow Visualization Society of Japan, Vol 3, No. 10, pp 71–74 (in Japanese)